Anal. Chem. **2007,** *79,* 1833−1839

Optimizing Micromixer Design for Enhancing Dielectrophoretic Microconcentrator Performance

Hsu-Yi Lee and Joel Voldman*

Department of Electrical Engineering and Computer Science, Massachusetts Institute of Technology, 50 Vassar Street, Room 36-824, Cambridge, Massachusetts 02139

We present an investigation into optimizing micromixer design for enhancing dielectrophoretic (DEP) microconcentrator performance. DEP-based microconcentrators use the dielectrophoretic force to collect particles on electrodes. Because the DEP force generated by electrodes decays rapidly away from the electrodes, DEP-based microconcentrators are only effective at capturing particles from a limited cross section of the input liquid stream. Adding a mixer can circulate the input liquid, increasing the probability that particles will drift near the electrodes for capture. Because mixers for DEP-based microconcentrators aim to circulate particles, rather than mix two species, design specifications for such mixers may be significantly different from that for conventional mixers. Here we investigated the performance of patterned-groove micromixers on particle trapping efficiency in DEP-based microconcentrators numerically and experimentally. We used modeling software to simulate the particle motion due to various forces on the particle (DEP, hydrodynamic, etc.), allowing us to predict trapping efficiency. We also conducted trapping experiments and measured the capture efficiency of different micromixer configurations, including the slanted groove, staggered herringbone, and herringbone mixers. Finally, we used these analyses to illustrate the design principles of mixers for DEP-based concentrators.

Rapid, highly sensitive detection and genetic analysis of pathogens are important goals for biotechnology. Polymerase chain reaction[1,2] is one commonly used method because of its potential for detecting a specific gene in a complex sample when there are less than 10 copies available. However, if sampling conditions have an adverse impact on the assay, the system may fail to detect a given pathogen in a small amount of concentrated liquid that is known to present a health risk. To improve the accuracy of pathogen detection, preconcentration and purification of a sample are often necessary. In addition, samples are often collected on a milliliter scale, whereas microscale pathogen detectors can only process samples on a microliter scale in a reasonable span of time. Thus, using a preconcentrator is useful for not only reducing the volume of the sample but also for retaining the pathogens for downstream analysis.

Among the existing approaches to preconcentration, microfluidic devices have attracted much attention since micro total analysis systems are becoming a focus for biomedical analyses. There are a number of sample preconcentration methods that are compatible with microscale detectors.[3−5] Among these methods, dielectrophoresis[6−8] (DEP)—the force on polarizable particles in nonuniform electric fields—has captured a lot of attention due to its ability to effectively trap, manipulate, and separate particles ranging from virus[9,10] to large DNA strands[11,12] to bacteria[13] and mammalian cells[14,15] in microfabricated devices.

A number of DEP-based microconcentrators have appeared in the literature, including approaches where the electric field is produced by arrays of insulating posts[1,16] or metal electrodes.[17−19] Among these, interdigitated electrodes (IDEs) are widely used because they are easy to fabricate, able to generate sufficiently strong electric fields with a reasonable voltage, and have an analytical electrical field solution available for modeling. However, because the magnitude of the DEP force decreases exponentially with distance above the electrodes,[20] IDE-based microconcentrators typically only sample a small portion of the input liquid stream unless the devices use shallow channels ($\ll$100 μm), operate at

* To whom correspondence should be addressed. E-mail: voldman@mit.edu. Fax: +1-617-258-5846. Tel: +1-617-253-2094.

(1) Barrett, L. M.; Skulan, A. J.; Singh, A. K.; Cummings, E. B.; Fiechtner, G. J. Microtechnology in Medicine and Biology. *3rd IEEE/EMBS Special Topic Conference*; 2005; pp 3−4.
(2) Call, D. R.; Borucki, M. K.; Loge, F. J. *J. Microbiol. Methods* **2003**, *53*, 235−243.
(3) Reyes, D. R.; Iossifidis, D.; Auroux, P.-A.; Manz, A. *Anal. Chem.* **2002**, *74*, 2623−2636.
(4) Vilkner, T.; Janasek, D.; Manz, A. *Anal. Chem.* **2004**, *76*, 3373−3386.
(5) Auroux, P.-A.; Iossifidis, D.; Reyes, D. R.; Manz, A. *Anal. Chem.* **2002**, *74*, 2637−2652.
(6) Voldman, J. *Annu. Rev. Biomed. Eng.* **2006**, *8*, 425−454.
(7) Pethig, R. *Crit. Rev. Biotechnol.* **1996**, *16*, 331−348.
(8) Gascoyne, P. R. C.; Vykoukal, J. V. *Proc. IEEE* **2004**, *92*, 22.
(9) Hughes, M. P.; Morgan, H. *J. Phys. D: Appl. Phys.* **1998**, *31*, 2205−2210.
(10) Green, N. G.; Morgan, H.; Milner, J. J. *J. Biochem. Biophys. Methods* **1997**, *35*, 89−102.
(11) Asbury, C. L.; Diercks, A. H.; Engh, G. v. d. *Electrophoresis* **2002**, *23*, 2658−2666.
(12) Chou, C.-F.; Tegenfeldt, J. O.; Bakajin, O.; Chan, S. S.; Cox, E. C.; Darnton, N.; Duke, T.; Austin, R. H. *Biophys. J.* **2002**, *83*, 2170−2179.
(13) Lapizco-Encinas, B. H.; Simmons, B. A.; Cummings, E. B.; Fintschenko, Y. *Electrophoresis* **2004**, *25*, 1695−1704.
(14) Rosenthal, A.; Voldman, J. *Biophys. J.* **2005**, *88*, 2193−2205.
(15) Taff, B. M.; Voldman, J. *Anal. Chem.* **2005**, *77*, 7976−7983.
(16) Cummings, E. B.; Singh, A. K. *Anal. Chem.* **2003**, *75*, 4724−4731.
(17) Dürr, M.; Kentsch, J.; Müller, T.; Schnelle, T.; Stelzle, M. *Electrophoresis* **2003**, *24*, 722−731.
(18) Gadish, N.; Voldman, J. *Anal. Chem.* **2006**, *78*, 7870−7876.
(19) Junya, S.; Ryuichi, Y.; Ryo, H.; Masanori, H. *J. Phys. D: Appl. Phys.* **1999**, *32*, 2814.
(20) Pethig, R.; Talary, M. S.; Lee, R. S. *IEEE, Eng. Med. Biol. Mag.* **2003**, *22*, 43−50.

10.1021/ac061647q CCC: $37.00
Published on Web 01/25/2007

low (<1 μL/min) flow rates, or both. To achieve higher flow rates while maintaining trapping performance, we have recently introduced a mixer-enhanced microconcentrator.[18] We used a patterned-groove chaotic micromixer[21] that creates complex flow profiles in the channel to bring more particles within proximity of the IDEs, increasing the percentage of particles that get trapped. Adding the mixer significantly increased the concentration enhancement at high flow rate (100−500 μL/min) compared to a concentrator without a micromixer.[18]

While we have quantitatively shown that adding a micromixer into the microconcentrator can increase the trapping efficiency of IDEs, the choice of the optimal micromixer configuration for this application has not been resolved. We note that the mixer is used here not to mix two species but rather to circulate the flow in order to bring particles close to the electrodes. Thus, the intuition and design rules developed for the patterned-groove mixers must be reevaluated in light of this new application.

Here we report on the properties of patterned-groove micromixers in order to optimize their geometry for enhancing DEP-based concentrator performance. We emphasize that our interest here is in describing the variations in performance of different *mixers*, not in the mechanics of DEP-based particle collection on IDEs, which has been adequately described in the literature.[22,23] First, we describe the development of modeling software for simulating particle trapping in mixer-enhanced DEP-based concentrators. Second, we describe an experimental methodology to measure the capture efficiency of different mixer configurations. Together, we use the modeling and experiments to evaluate different micromixers, providing a better understanding of which micromixer geometries are optimal for microconcentrators.

EXPERIMENTAL SECTION

Device Fabrication and Packaging. The device fabrication and packaging details have been described previously.[18] Briefly, we pattern gold interdigitated electrodes on a Pyrex wafer (Bullen Ultrasonics, Eaton, OH). The width and spacing of the electrodes are both 20 μm. We cast PDMS into an SU-8 mold to make the micromixers. The micromixers consist of a 500 μm × 200 μm × 35 mm (width × height × length) channel on the bottom and 100-μm-high grooves on the top. We then package the IDE chip and micromixer on a PCB board to integrate with the fluidics and electronics.

Fluidics. We use plastic syringes loaded with water and 1% Alconox detergent (Alconox, White Plains, NY) and driven by a syringe pump (KD Scientific 200, Holliston, MA). The syringe pump controls the flow rate of liquid through the device. Between the syringes and the device, we use two valves to manage the input media and sample. Valve 1 switches the media between water and detergent solution, and valve 2 controls the sample loading/injection.

Electronics. We used a function generator (33220A, Agilent, Palo Alto, CA) to provide electrical excitation to the device. An oscilloscope (Tektronix, Richardson, TX) was used to monitor the voltage across the channel.

Sample Preparation. We used 1-μm-diameter fluorescent pink Carboxyl magnetic microspheres (Spherotech, Libertyville, IL) in 1% w/v suspension (~1×10^{10} beads/mL) with a density of 1.050 g/cm^3. While the beads used in the experiments are magnetic, they were selected because of their size; their magnetic properties have no effect on DEP trapping. We resuspended beads with DI water to approximately the desired concentration (10^5−10^6 bead/mL) and measured the exact concentration with a hemacytometer (VWR, Cambridge, MA). We also measured suspension conductivities to be ~5×10^{-4} S/m using a Thermo Orion model 555A conductivity meter (VWR, Cambridge, MA).

Experimental Protocol. The experimental protocol starts by flushing the channel with DI water at high flow rate to eliminate bubbles in the channel. After the channel is degassed, we apply 100 kHz, 20 V_{pp} to the electrodes to initiate trapping and introduce the bead sample into the channel at a 200 μL/min flow rate. When the full volume of the sample (100 μL) has flowed through the device, we stop the flow and plug the outlet. For easier observation of beads and more precise image counting (see below), we deactivate the DEP force and let the beads diffuse. After sufficient diffusion time (~20 s), we take pictures along the whole channel. After one experiment, we deactivate DEP and flow detergent solution into the channel to release the trapped beads. The micromixer is detachable from the device, so we can use the same set of interdigitated electrodes repeatedly with different micromixers, eliminating variation due to fabrication nonuniformities across different electrode chips.

Imaging. We observed the devices with an automated Zeiss Axio imager reflected-light microscope (Zeiss, Thornwood, NY). We used a Sensicam QE cooled-CCD digital camera (The Cooke Corp., Romulus, MI) with a green filter set (31000, Chroma, Long Beach, CA) to obtain fluorescent images.

Quantitative Image Analysis. We counted the number of beads in each image using custom image-processing software. The software has three main functions: image preprocessing, converting intensity images to binary images, and counting objects. The first function preprocesses the image by subtracting background and enhancing contrast to achieve better counting results. Then it converts the intensity image into a binary image (see Figure S1 Supporting Information). Finally, it quantifies the number objects in the binary image. While counting the objects, we encountered one challenge. Beads that touched each other were counted as one object and thus were indistinguishable from single beads. To overcome this challenge, we first deactivated the DEP force while taking images to decrease the magnitude of bead aggregation (Figure 1A, B). This improves measurement accuracy, especially at high concentration (Figure 1C). Then we used algorithms to detect abnormally sized objects and estimate the number of beads within by dividing the object area by the mean bead size in the image. Our final image-counting algorithm has <10% error over the tested range of bead concentrations.

RESULTS

The fabricated device contains two major components: IDEs and a micromixer, as illustrated in Figure 2A. On the bottom, the IDEs generate positive DEP to collect particles in the passing flow. On the top, the micromixer—a flow channel with grooves—circulates the flow to expose more particles to the DEP effective region (Figure 2B).

(21) Stroock, A. D.; Dertinger, S. K. W.; Ajari, A.; Mezić I.; A. Stone, H.; Whitesides, G. M. *Science* **2002**, *295*, 647−651.
(22) Holmes, D.; Green, N. G.; Morgan, H. *IEEE, Eng. Med. Biol. Mag.* **2003**, *22*, 85−90.
(23) Becker, F. F.; Wang, X. B.; Huang, Y.; Pethig, R.; Vykoukal, J.; Gascoyne, P. R. C. *Proc. Natl. Acad. Sci. U.S.A.* **1995**, *92*, 860−864.

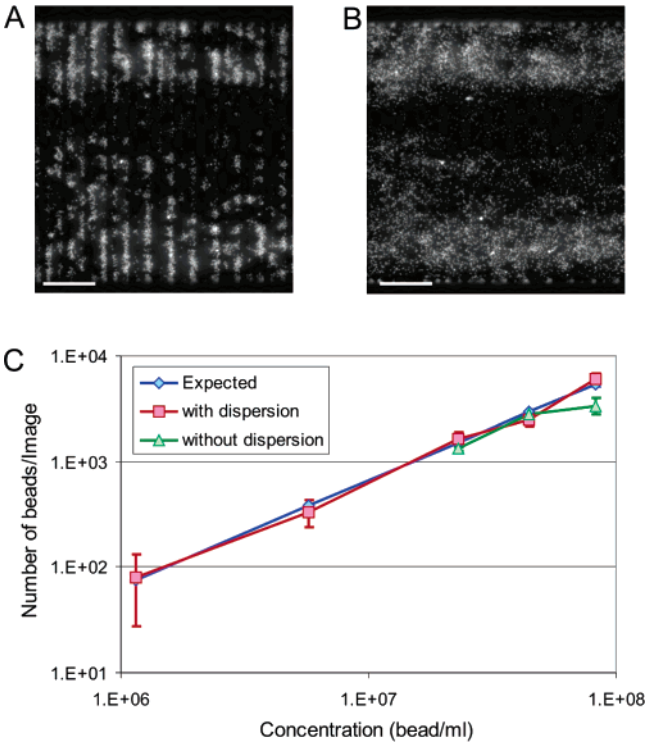

Figure 1. Measuring bead concentration. (A) A fluorescence image of trapped beads with the DEP force activated. (B) A fluorescence image of beads after the DEP force is turned off, showing the beads dispersing. The scale bar represents 200 μm. (C) Measured number of beads compared to the expected value as the input bead concentration varies. Allowing the beads to disperse results in more accurate counts at higher bead concentration.

A particle in the device experiences the DEP force, the hydrodynamic (HD) drag force, and other minor forces: the gravitational force, the HD lift force, and normal forces from the top and bottom of the flow chamber. The net force exerted on a particle determines the particle motion in the device and whether a particle is trapped or not. In order to predict the particle trapping and evaluate mixer numerically, we used custom software to model these forces and simulate the particle motion resulting from these forces. The software is an extended version of the one developed by Rosenthal et al.[24] for simulating multiple forces exerted on a single particle in a microfluidic system. Specifically, we extended the software to calculate not only the DEP force generated by arbitrarily shaped electrodes but also HD forces produced by complex fluid geometries. It accepts electric field solutions, fluid flow-field solutions, and particle information as inputs and calculates the total force exerted on a particle everywhere in the space.

We obtained the nonuniform electric field generated by the interdigitated electrodes by using the closed-form analytic solution of the electric field derived by Chang et al.[25] The obtained 2-D solution is repeated along the interdigitated array to form a 3-D electric field. We solved for the fluid flow field in the micromixer using the commercial field solver Comsol Multiphysics (Comsol, Inc. Burlington, MA). As shown in Figure 3, three kinds of micromixers were simulated: the slanted groove micromixer (SGM), the herringbone micromixer (HM), and the staggered herringbone micromixer (SHM). Only one period of each micromixer (12 grooves) was modeled, and pressure boundary conditions were used at the ends of the channel. The solved velocity field was then exported to Matlab (R14, The Mathworks Inc., Natick, MA) and mapped onto a regular Cartesian grid. We then scaled the fluid flow field to the desired flow rate. Finally, we formed the flow profile for the full mixer by repeatedly cascading the solution obtained for one period. To verify the flow pattern obtained by Comsol Multiphysics, we compared the calculated flow profiles with those obtained by different numerical schemes[26] or experiments[21] (data not shown) and found them to be in agreement.

We imported the calculated electric field and fluid flow field into the modeling software and computed the force exerted on a particle as described previously.[24,27] Due to the small mass of the particles, we ignored particle inertia and assumed the system was in quasi-steady state. Therefore, the particle responds to the force instantaneously and its movement follows the direction of the net force. Based on the above assumption, the particle path is the same as the streamline of the force field. We also assume that all the forces are exerted on the center of the particle and that the particle is much smaller than the fluidic/electric field nonuniformities, so that we may neglect particle rotation. Finally, we neglect any particle−particle interactions; particles will not feel the fluid flow field and electric field distorted by nearby particles.

Figure 3 shows the computed trajectories for four particles starting at the same height from the beginning of the channel.

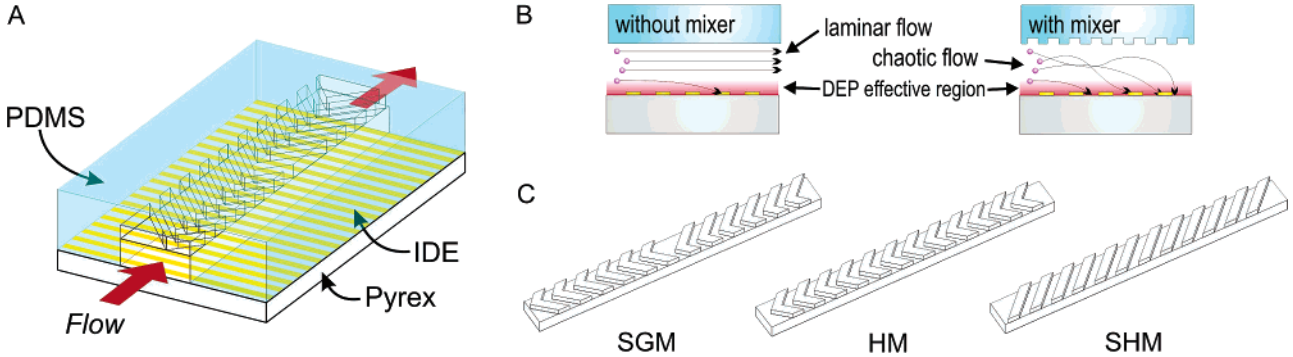

Figure 2. Device overview. (A) Illustration of the assembled devices, showing the PDMS channel and gold IDEs on the Pyrex substrate. (B) Illustration of particle trapping in laminar flow and chaotic flow. Without the mixer, only a portion of particles carried by the laminar flow are exposed to DEP and trapped by electrodes. Chaotic flow generated by a passive micromixer circulates the particles and exposes more particles to the DEP region. (C) Schematic of the three kinds of micromixer geometries described in this work. From left to right: slanted groove micromixer (SGM), herringbone micromixer (HM), and staggered herringbone micromixer (SHM).

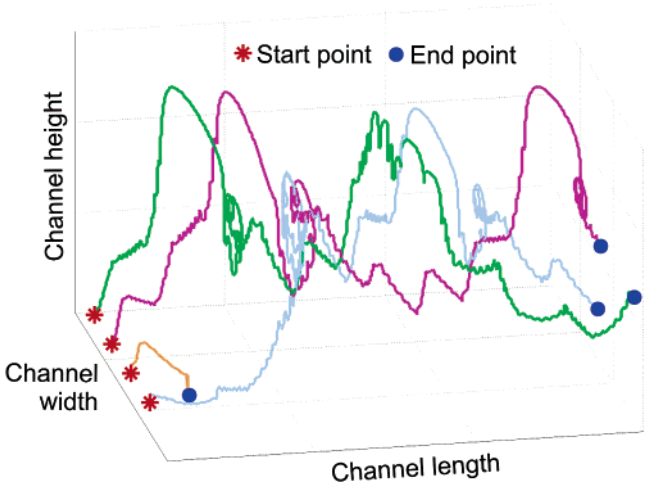

Figure 3. Simulated trajectories of particles in the SHM. Four particles start at the beginning of the mixer. One particle is trapped by the electrodes, while the others exit the channel. Simulation parameters are as described in the text except that the electrode width and spacing are 20 μm.

The spiraling trajectories show the effect of the mixer, and the blue points represent the final location where the particles terminate. If the trajectory ends on the bottom plane, it means that the particle is trapped by DEP. Conversely, if the trajectory finishes at the end of the channel, it means the particle passes the whole channel without being trapped. By counting the percentage of the trapped particles, the program can determine what percentage of the particles is trapped by different mixers and thus each mixer's trapping efficiency.

In order to understand how different micromixers circulate particles, we plot particle trajectories within each mixer when the electric field is turned off. Figure 4 shows the trajectories of two representative particles in different micromixers with the axis of the channel pointing into the page. We see that the different mixers create qualitatively different circulating profiles. In the SGM (Figure 4 left), particles travel in coincident trajectories around the centerline. As long as the groove geometry remains the same, particles will circulate around fixed orbits and there will be no mixing between the inner and outer particles. These trajectories are effective for trapping particles near the walls of the channel, because they have sufficient chance of approaching the bottom of the channel where the DEP force is strong. However, particles near the interior of the channel will not travel near the electrodes and thus are unlikely to be collected by the concentrator. A similar situation occurs in the HM except that the circulation has two rotation centers on each side instead of having one in the middle (Figure 4, middle).

The SHM, meanwhile, creates an irregular mixing pattern (Figure 4, right). Its asymmetric herringbone grooves generate two circles of flow, but the circles are different in size. In addition, for every half circle, the centers of the circles exchange their positions due to the change in the position of the asymmetric herringbone tip. The change of the rotation center makes one lobe of fluid transfer to the other side. Therefore, every half cycle, the flow reconstructs and some particles have a chance to switch to the other orbits every half cycle. This asymmetric geometry makes the particle trajectories more irregular, thus maximizing the exposure of particles to the DEP.

After understanding the mixing pattern created by micromixers, we factored in the effect of DEP and performed simulations and experiments to measure particle trapping. The simulations used the following parameters: particle diameter 1 μm, bead density 1050 kg/m^3, liquid density 1000 kg/m^3, CM factor 0.8, applied voltage 20 V_{pp}, flow rate 200 μL/min, and electrode width and spacing 16 and 24 μm, respectively, to match the experiment conditions. In the simulation, we started 1000 beads at random locations at the beginning of the channel and colored them on each side differently in order to show the effect of micromixers.

We present the top view of fluorescent images of the trapped bead distribution and the simulated trapped particle distribution in Figure 5. The particles in the smooth channel are mostly trapped at the beginning of the channel and the number of trapped particles decreases significantly along the channel (Figure 5A). Nevertheless, with micromixers, particle trapping is dramatically increased, and over multiple experiments and simulations, we observed that the bead/particle distributions consistently exhibited distinctive patterns corresponding to the type of micromixer used in the device. The particles in the SGM appear distributed close to the side of the channel (Figure 5B). In contrast, in the HM (Figure 5C) and SHM (Figure 5D), fewer particles are trapped around the centerline. The simulated captured particle distributions closely mirror the experimentally obtained images. We can explain the observed particle distributions with reference to our results in Figure 4. Here we see that during circulation particles in the SGM stream upward on one side of the channel, whereas in the HM and SHM they stream upward in the middle of the channel. This lifting flow works against the downward DEP trapping force, and thus may explain the observed lack of particles on the side (SGM) and center (HM and SHM) of the channels.

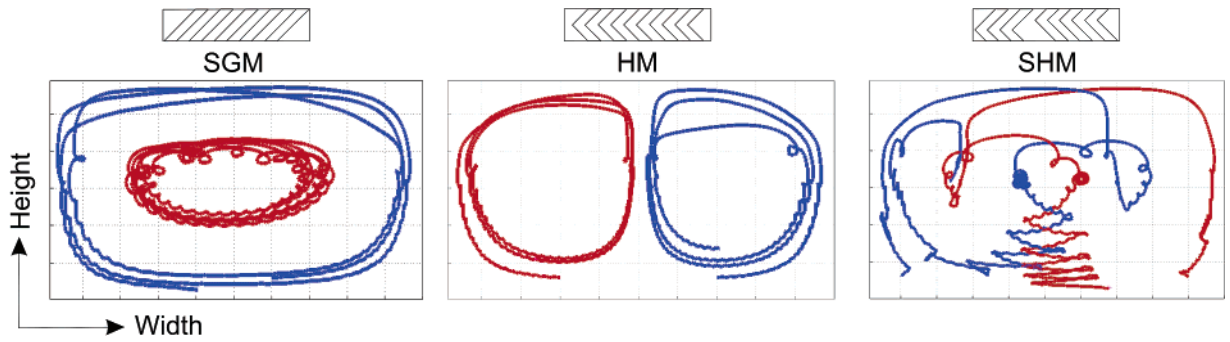

Figure 4. Mixing pattern in the different micromixers. Plotted are cross sections of two representative particle trajectories in the SGM (left), HM (middle), and SHM (right) to show the different mixing behaviors. Top views of corresponding micromixer geometries are shown above each plots.

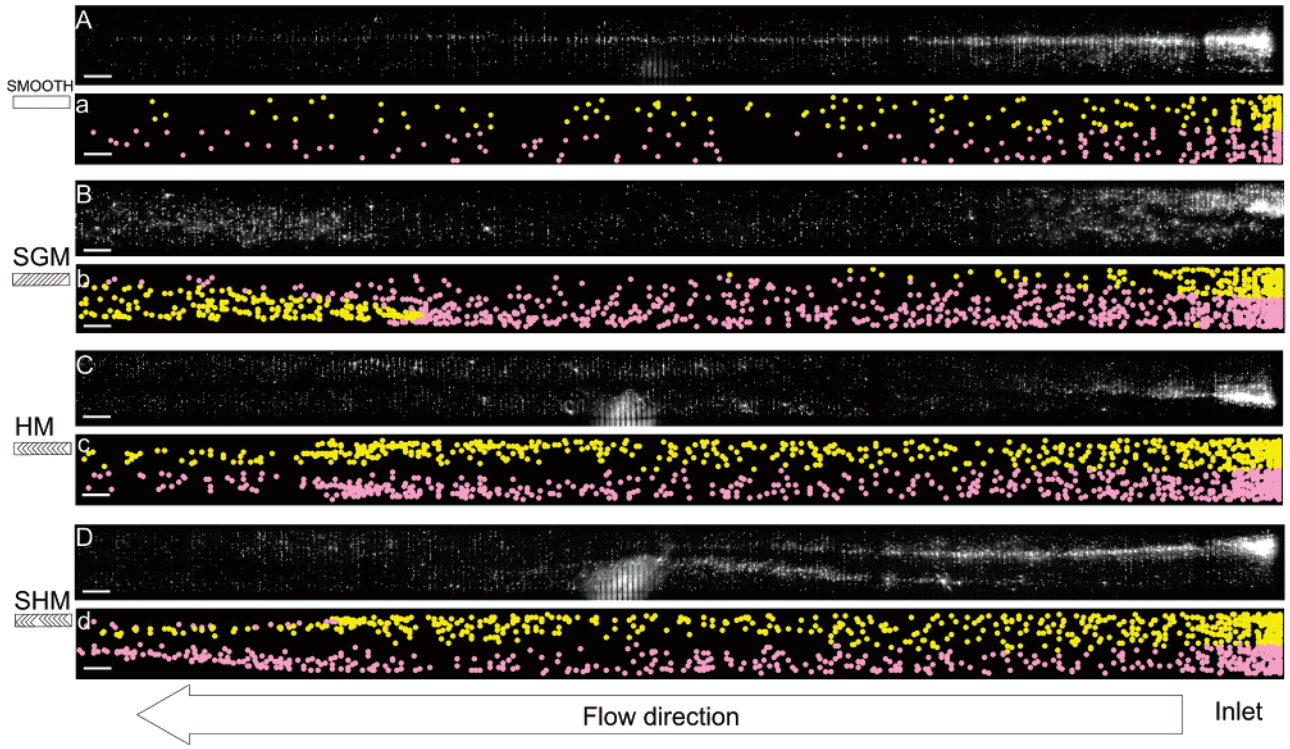

Figure 5. Top view of the trapped beads along the channel in the smooth (A,a), SGM (B,b), HM (C,c), and SHM (D,d). Simulated distribution results (a−d) are plotted alongside the experimental images (A−D). The scale bars represent 200 μm. The bead size is not to scale.

Moreover, the particle-free strip meanders around the centerline in the SHM, which can be explained by noting that the asymmetric geometry of the SHM changes the position of the lifting flow.

The effects of the micromixers are also evident in the distribution of the differently colored beads in the simulations. In the smooth channel (Figure 5a), beads of two colors remain on the same side. In the SGM, the two colors appear in turn (Figure 5b) because the two streams are twisted and sent to the bottom one at a time. In HM, beads of the same color remain on the same side because the mixing pattern consists of two individual circles (Figure 5c). In SHM, the color beads can cross the centerline and get trapped on the other side due to the chaotic mixing mechanism (Figure 5d).

In order to quantitatively evaluate the performance of each micromixer in aiding particle trapping, we defined trapping efficiency as [number of beads trapped]/[number of input beads]. In the experiments, the number of trapped beads is calculated using quantitative image analysis and the number of input beads is determined from the input bead concentration and the input sample volume. We repeated the experiments with various input sample concentrations (10^5−10^6 bead/mL). Among all micromixers (Figure 6A), the SHM exhibits the greatest trapping efficiency, while the smooth channel always remains the lowest. The performance of the other two micromixers (SGM and HM) is in the middle. We noticed that the performance results varied across the different experiment runs (and thus input particle concentrations). This is likely due to error in the measured input bead concentration. However, we emphasize that even with the inter-experiment variation, the relationship among the mixers always remains the same and the trapping efficiency shows no significant dependence on the input concentration over the range measured.

Inspired by the mixing characteristics of SGM and HM, we created a mixer combination: SGM + HM. SGM + HM has slanted grooves in the first half of the channel and centered herringbone grooves in the second half. This combination should have better performance than the pure SGM because in the HM section the mixing pattern can pull out the middle particles that are isolated by the SGM section. A comparison of experimental results using the pure SGM and hybrid SGM + HM is shown in Figure 6B, which illustrates the trapped bead distribution along the channel. In the first half of the channel, SGM and SGM + HM exhibit a similar trapping efficiency. The number of the trapped beads decreases along the channel length because most of the particles in the outer circles are gradually trapped. However, in the second half of the channel, while SGM still has a decreasing number of trapped beads, SGM + HM increases the number of trapped beads dramatically due to the change in mixing pattern. Over six experiments, the increase of the trapped beads consistently occurred right after the fluid entered the HM section. This was also reflected in measurements of trapping efficiency, where the SGM + HM consistently exhibited improved trapping efficiency as compared to the SGM (Figure 6A). These data support the notion that using the HM after the SGM exposes more particles in the middle of the channel to the DEP region and hence can increase the number of trapped particles.

In Figure 6C, we show a comparison between the averaged experimental results of Figure 6A and simulation results. The

(24) Rosenthal, A.; Taff, B. M.; Voldman, J. *Lab Chip* **2006**, *6*, 508−515.
(25) Chang, D. E.; Loire, S.; Mezić, I. *J. Phys. D : Appl. Phys.* **2003**, *36*, 3073−3078.
(26) Kang, T. G.; Kwon, T. H. *J. Micromech. Microeng.* **2004**, *14*, 891−899.
(27) Voldman, J.; Gray, M. L.; Toner, M.; Schmidt, M. A. *Anal. Chem.* **2002**, *74*, 3984−3990.

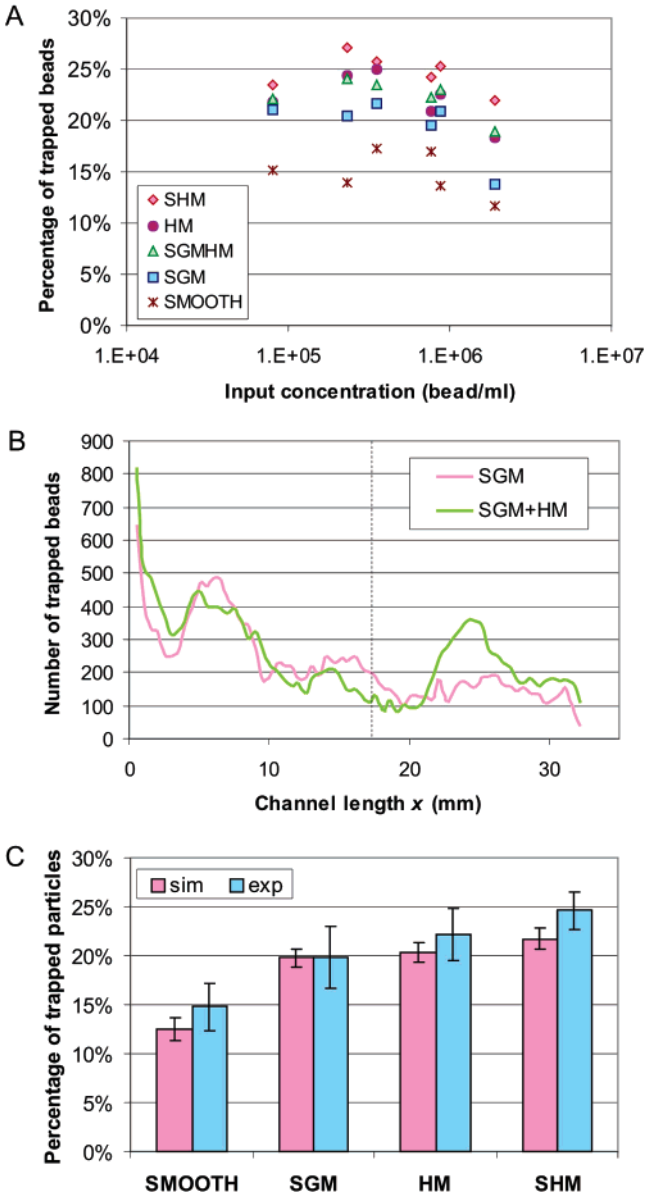

Figure 6. Trapping results. (A) Measured trapping efficiencies for the different mixers with varying input bead concentration. (B) Measured number of trapped beads along the channel for both the SGM and SGM + HM configurations. The dashed line denotes the start of the HM section for the SGM + HM configuration (slanted grooves persist after the dashed line in the SGM configuration). An apparent increase in the number of trapped beads occurs in SGM + HM after the dashed line. (C) Comparison of simulated and experimental trapping efficiency. The fabricated devices have 16-mm-wide electrodes with 24-mm spacing and a groove-to-channel aspect ratio of 0.22 (SGM), 0.23 (HM), and 0.25 (SHM).

simulations account for the as-fabricated dimensions of the device, including the width of electrodes and the aspect ratio of the groove to the channel. The error bars in the simulations are obtained by repeating the same simulation with particles starting at random points. The simulation results agree with the experimental results. Both demonstrate that adding any type of circulating flow to a smooth channel will increase the trapping efficiency. The experimental data (Figure 6A) suggest that the SHM is more efficient than the SGM and HM. The simulations show an insignificant difference between the three mixers. This is likely due to inaccuracies in the simulations resulting from mesh-size sensitivity and interpolation errors. Additionally, simulation simplifications such as neglecting particle−particle interactions, or the irregular drag force near the wall, may account for mismatches between experiments and simulations. Remarkably, though, the simulations absolutely match the experiments to within the errors of each, even though no fitting parameters are used.

The nature of our experiments, which are concerned with the variation in performance of different mixers, intrinsically provides controls for several potentially important phenomena. ac electroosmosis (ACEO), where the electric fields couple with charge to induce recirculating flows,[28] is unlikely to be significant in our experiments because it would affect all four channels equally, yet we still observe differences among them, especially between the smooth channel and the corrugated ones. Further, our simulations, which do not include ACEO, match our experiments to within error, suggesting that ACEO is not important, and we did not experimentally observe ACEO in the smooth channel, where it would be most apparent. Finally, simple scaling calculations suggest that ACEO effects are 1000× smaller than DEP under our conditions. Similar arguments can be made for other potential experimental artifacts, such as changes in solution conductivity.

DISCUSSION

We have verified that a micromixer can produce a helical flow (circulation) and increase the trapping efficiency of IDE-based DEP microconcentrators. Since micromixers for DEP-based microconcentrators are intended to circulate particles and bring them in proximity with the IDEs, rather than for mixing two particle populations, the criteria used to design and judge the optimal micromixer will be different from those used for conventional micromixers.[29]

First, to be able to integrate with IDEs, one requires a micromixer that can be easily fabricated. State-of-the-art micromixers can be categorized either as passive micromixers or as active micromixers according to the ways that they generate disturbance.[30] Active micromixers usually consist of components, such as a pump, valve, or electrode, which are often complicated in structure and require external energy. On the other hand, passive micromixers do not require any external energy except a pressure difference to drive the flow. For easy integration with IDE arrays, passive micromixers are more appropriate.

Second, due to the requirement of concentration enhancement, the particles should be trapped in a total chamber volume smaller than the input sample volume. The concentration enhancement is defined as [output concentration]/[input concentration], and on-chip concentration is defined as [number of beads trapped]/[chamber volume]. Thus, decreasing the chamber volume will directly increase the concentration enhancement. However, a small chamber volume will cause high flow velocity and hence negatively affect DEP trapping. Therefore, an optimal chamber volume exists.

Third, generating vertical flow is more important than achieving even mixing. Since the electrodes are on the bottom of the channel and the DEP forces decay exponentially with height, the

(28) Castellanos, A.; Ramos, A.; Gonzalez, A.; Green, N. G.; Morgan, H. *J. Phys. D : Appl. Phys.* **2003**, *36*, 2584−2597.
(29) Ottino, J. M.; Wiggins, S. *Science* **2004**, *305*, 485−486.
(30) Nguyen, N. T.; Wu, Z. *J. Micromech. Microeng.* **2005**, *15*, R1−R16.

simplest way to increase the trapping efficiency is to bring particles near the ceiling of the channel down by circulating the flow. Thus, micromixers with poor mixing performance in the conventional sense (Figure S2 Supporting Information), such as SGM and HM, are still able to generate helical flow to enhance trapping and hence are appropriate micromixers for microconcentrators. However, other micromixers, such as those which mix two species injected from each side of a Y-shape inlet,[31−34] but lack circulation in the *z*-direction, are less appropriate for aiding DEP-based trapping.

Finally, among patterned-groove micromixers where vertical flow exists, we found that chaotic mixing helps expose more particles to the DEP field than nonchaotic mixing, which means that it can achieve a higher trapping efficiency. For example, staggering herringbones or adding a HM behind the SGM to change the mixing pattern are ways to generate chaos and result in trapping efficiencies higher than the nonchaotic SGM and HM. Therefore, with the third condition where vertical flow exists, a chaotic micromixer is preferred.

One outstanding question is whether the results we have obtained hold at low input particle concentrations, since real-world applications often require operating with particle concentrations down to the 10^3/mL range (or lower). We expect that the variations among the different mixers will hold at low input concentrations and that circulating flows will always improve trapping efficiency for the simple reason that they bring more particles in proximity to the electrodes. In addition, DEP-based microconcentrators tend to perform worse at higher input concentrations where particle saturation starts to occur[18] but have no equivalent effects at low input particle concentrations. Indeed, the simulations effectively model single particles traveling through the device and, thus, very low concentrations. Because they match the experiments, one would expect the experimental results to be valid down to those low concentrations.

CONCLUSIONS

We have presented simulation and experiments on micromixer-enhanced DEP-based microconcentrators. We created modeling software that takes a user-supplied complex fluid flow field and predicts the particle motion in these devices. We have shown that the modeling software provides useful insight into how micromixers affect DEP-based trapping. We also developed an imaging-based experimental method for demonstrating the quantitative performance of fabricated devices. Our results demonstrate that the optimal grooved micromixer is the staggered herringbone mixer, which enhances trapping efficiency by ~1.5× as compared to a smooth channel.

ACKNOWLEDGMENT

We thank Mike Vahey for helpful discussions and the MIT Microsystems Technology Laboratories (MTL) for fabrication support. This work was supported by Draper Laboratories and National Aeronautics and Space Administration (NASA).

SUPPORTING INFORMATION AVAILABLE

Additional information as noted in text. This material is available free of charge via the Internet at http://pubs.acs.org.

Received for review September 1, 2006. Accepted December 14, 2006.

AC061647Q

(31) Mengeaud, V.; Josserand, J.; Girault, H. H. *Anal. Chem.* **2002**, *74*, 4279−4286.

(32) Wong, S. H.; Bryant, P.; Ward, M.; Wharton, C. *Sens. Actuators, B* **2003**, *95*, 414−424.

(33) Lin, Y.; Gerfen, G. J.; Rousseau, D. L.; Yeh, S.-R. *Anal. Chem.* **2003**, *75*, 5381−5386.

(34) Sudarsan, A. P.; Ugaz, V. M. *Proc. Natl. Acad. Sci. U.S.A.* **2005**, *103*, 7228−7233.